Slip length of water on graphene: Limitations of non-equilibrium molecular dynamics simulations

Sridhar Kumar Kannam, B. D. Todd, J. S. Hansen, and Peter J. Daivis

Related Articles

In situ imaging of orthoclase–aqueous solution interfaces with x-ray reflection interface microscopy
J. Appl. Phys. 110, 102211 (2011)

Interaction between water and defective silica surfaces
J. Chem. Phys. 134, 114703 (2011)

Pressure cell for investigations of solid–liquid interfaces by neutron reflectivity
Rev. Sci. Instrum. 82, 023902 (2011)

Communication: Molecular dynamics simulations of the interfacial structure of alkali metal fluoride solutions
J. Chem. Phys. 133, 061103 (2010)

Effects of nanofluids containing graphene/graphene-oxide nanosheets on critical heat flux
Appl. Phys. Lett. 97, 023103 (2010)

Additional information on J. Chem. Phys.

Journal Homepage: http://jcp.aip.org/

Journal Information: http://jcp.aip.org/about/about_the_journal

Top downloads: http://jcp.aip.org/features/most_downloaded

Information for Authors: http://jcp.aip.org/authors

Slip length of water on graphene: Limitations of non-equilibrium molecular dynamics simulations

Sridhar Kumar Kannam,[1,a)] B. D. Todd,[1,b)] J. S. Hansen,[2,c)] and Peter J. Daivis[3,d)]

[1]*Mathematics Discipline, Faculty of Engineering and Industrial Science and Centre for Molecular Simulation, Swinburne University of Technology, Melbourne, Victoria 3122, Australia*
[2]*DNRF Center 'Glass and Time', IMFUFA, Department of Science, Systems and Models, Roskilde University, DK-4000, Roskilde, Denmark*
[3]*School of Applied Sciences, RMIT University, Melbourne, Victoria 3001, Australia*

Data for the flow rate of water in carbon nanopores is widely scattered, both in experiments and simulations. In this work, we aim at precisely quantifying the characteristic large slip length and flow rate of water flowing in a planar graphene nanochannel. First, we quantify the slip length using the intrinsic interfacial friction coefficient between water and graphene, which is found from equilibrium molecular dynamics (EMD) simulations. We then calculate the flow rate and the slip length from the streaming velocity profiles obtained using non-equilibrium molecular dynamics (NEMD) simulations and compare with the predictions from the EMD simulations. The slip length calculated from NEMD simulations is found to be extremely sensitive to the curvature of the velocity profile and it possesses large statistical errors. We therefore pose the question: Can a micrometer range slip length be reliably determined using velocity profiles obtained from NEMD simulations? Our answer is "not practical, if not impossible" based on the analysis given as the results. In the case of high slip systems such as water in carbon nanochannels, the EMD method results are more reliable, accurate, and computationally more efficient compared to the direct NEMD method for predicting the nanofluidic flow rate and hydrodynamic boundary condition. © *2012 American Institute of Physics.* [doi:10.1063/1.3675904]

I. INTRODUCTION

Recent developments in nanoscience and nanotechnology have enabled the fabrication of nanofluidic devices such as micro/nano electro-mechanical systems, nanopipettes, nanobiosensors, nanomotors, lab-on-a-chip devices, etc.[1] As these devices have unique attributes such as nanoliter capacity, low energy dissipation, high accuracy and sensitivity, and enhanced flow rates, understanding the physics of fluids at the nanoscale is very important in designing, fabricating, optimizing, and utilizing these devices. Gravity and inertia effects which may play a dominant role at the macroscale are negligible at the nanoscale and new phenomena due to the high surface to volume ratio emerge.[2] Transport of momentum and energy become non-local in nature[3,4] and the molecular behavior at the fluid-solid interface profoundly affects the transport.[5,6] Theoretically, continuum based approximations may be invalid or difficult to formulate at the nanoscale[7] and experimental difficulties are also not yet fully solved.[8] Computer simulations of the type used in the present study have therefore become a viable tool for studying nanoscale phenomena.

Starting from the last decade, water confined in carbon nanostructures has received significant attention due to the importance of water and the unique properties of carbon.[9–43]

A number of studies have been aimed at quantifying the slip length and flow rate of water in carbon nanotubes (CNTs) and flat graphene nanochannels, both experimentally[12–19] and in simulations.[21–38] However, the data are widely scattered: even over orders of magnitude and no consensus has been reached. Water has been shown to have almost a plug like velocity profile, resulting in 1 to 5 orders of magnitude flow enhancement compared to classical Navier-Stokes prediction assuming a no-slip boundary condition (BC). Qualitatively, some studies have found a very high slip length in very small diameter CNTs and as the tube diameter increases, the slip length approaches a constant value which is equal to the slip length on a flat graphene surface.[29,32,33,43] Contrary to this, some researchers have found the opposite behavior and attribute this to the increase in surface friction as the tube diameter is decreased.[23–25] In a very recent field effect transistor experimental study, Qin *et al.*[18] found non-monotonic behavior of slip, which has also been reported by Sokhan *et al.*[44] for slip of methane in CNTs. Hence, even qualitatively we have contradictory slip behavior in CNTs.

In experimental studies, Maali *et al.*[17] found a slip length of 8 ± 2 nm for water on a graphite surface. Qin *et al.*[18] found a decreasing slip length as the CNT diameter is increased from 0.81 to 1.59 nm with a non-monotonic behavior at 1.08 nm diameter tube. As the tube diameter increases to 1.59 nm, its slip length converges to 10 nm, which can be approximated to the slip length of water on planar graphene. Zhu and Granick[45] and Tretheway and Meinhart[46] found micrometer range slip lengths for water on hydrophobic surfaces. In

---

a)Electronic mail: urssrisri@gmail.com.
b)Electronic mail: btodd@swin.edu.au.
c)Electronic mail: jschmidt@ruc.dk.
d)Electronic mail: peter.daivis@rmit.edu.au.

simulations, Thomas and McGaughey[29] found 30 nm, Falk *et al.*[32] found 80 nm, and Kotsalis[34] found 67 ± 45 nm slip lengths for water on graphene surfaces. Babu and Sathian[33] found monotonically decreasing slip length as the tube diameter is increased from 0.81 to 5.42 nm and in the higher diameter tubes the slip length converges to just about 1 nm, which can be taken as the slip length on a flat graphene surface. Some of this variation can be attributed to the difference in water models and carbon models used in simulations. Theoretically, Myers[43] predicted 39 nm slip length in the limit of high diameter CNTs. As explained by Kotsalis[34] the large uncertainties (67 ± 45 nm) are due to the large variation in the velocity gradient of water at the graphene surface. Thomas and McGaughey[29] calculated the viscosity of confined water in equilibrium molecular dynamics (EMD) simulations by using the Einstein self-diffusion coefficient and they used this viscosity to constrain the fit to the non-equilibrium molecular dynamics (NEMD) streaming velocity profiles. They found that unconstrained fits result in almost 100% variation in the predicted slip length and the viscosity of water.

Experimentally, fabricating a perfect defect free individual carbon nanotube is extremely difficult. Moreover measuring the tube diameter, controlling the pressure difference to drive the fluid, and finally performing the nanoliter volume experiment is a cumbersome procedure, which could be one reason for the scattered data in experiments.[12–19] In simulations, the commonly used NEMD methods also have their limitations. At room temperature water has an average thermal velocity of 340 m/s and the fluid velocities in experiments are on the order of 0.01 m/s. NEMD simulations can only simulate the systems for a few nanoseconds with a time step of ~1 fs. Due to this computational limitation, NEMD simulations are done with very high pressure gradients (or shear rates in Couette flow) to obtain a mean fluid velocity comparable to the thermal velocity and thus statistically significant results. At these high fields nonlinear effects may begin to emerge and the slip length diverges.[47] Therefore, the extrapolation of NEMD results to experimental fields is not reliable and is likely to lead to deviation from the flux determined under experimental conditions, where the hydrodynamic properties obey linear relations.[41] Moreover, to do the extrapolation these NEMD simulations have to be performed for a range of pressure gradients or shear rates. In order to reduce the computational time and thus avoid the complex carbon models, a number of studies freeze the carbon atoms to their lattice sites and thermostat the water directly to maintain the desired temperature. It has been shown that the molecular momentum transfer at the fluid-solid interface plays a key role in nanofluidic behavior as the fluid transport properties are dominated by the interface.[5,44,48] Indeed, thermostatting the fluid instead of the walls can lead to unphysical distortions of the fluid's stress response and can artificially enhance or reduce the slip, depending on the type of wall surface.[44,48] Sokhan *et al.*[44,49] observed an increase of ~20% in slip for methane in flexible graphene/CNTs compared to rigid counterparts. Refer to our previous work for a broader discussion.[47] It is however worth pointing out here that a systematic study of the effects of wall roughness, frozen vs vibrating walls (and correspondingly, thermostatting the fluid vs thermostatting the

walls), and the various *ab initio* slip models is yet to be accomplished and would represent a very useful study in the field. For example, the recent publication by Groombridge *et al.*[37] uses the equilibrium model of Sokhan and Quirke[50] to study the slip of water confined by amorphous surfaces of carbon and polydimethylsiloxane and finds reasonable agreement between NEMD and EMD results (see their Table 1).

For high slip systems such as water against a hydrophobic surface, the problem becomes even more complicated. As mentioned above, and as we will show in Sec. III, a very small change in the measured NEMD velocity profile can result in a very large deviation in the slip length. This suggests the need for developing new theoretical methods for the prediction of such a highly sensitive phenomenon. Recently, Hansen *et al.*[51] proposed a method of calculating the intrinsic friction between fluid and solid using EMD simulations based on a statistical mechanical approach. The method has successfully predicted the slip length for atomic fluids and methane confined between Lennard-Jones solid walls[51] and inside graphene nanochannels.[47] Our preliminary results of methane flow in CNTs show that the minimum slip length for any diameter CNT is greater than or at least equal to the slip length on a flat graphene surface.[52] Understanding the behavior of water on a flat graphene surface and documenting its slip length is crucial before we completely understand the behavior in CNTs which are a cylindrical form of graphene, where the curvature of the tube affects the friction. This is the motivation of the present study. In this work using EMD simulations (with no pressure gradient or shear rate), thus bypassing limitations of NEMD methods, we calculate the interfacial friction coefficient between water and graphene. Using this friction coefficient we determine the slip length and flow rate. We also perform NEMD simulations of Poiseuille and Couette flows for a wide range of external fields and shear rates to understand the slip phenomena further and compare these results to our EMD method predictions.

II. SIMULATION DETAILS

We use the recently parameterized flexible simple point charge (SPC/Fw) model for water, which reproduces the dynamical properties of water close to experimental values.[53–55] Graphene is modeled using the second generation reactive empirical bond order Tersoff-Brenner potential, which is widely used for carbon allotropes.[56] Electrostatic interactions between water molecules are modeled using the Wolf method,[29,30,55,57,58] which enables us to simulate for longer times and 20 simulations at each state point. The interaction between water molecules and carbon atoms of the graphene is modeled using the Lennard-Jones potential with parameters of Werder *et al.*[42] We have used two layers of graphene at two walls to produce a stable system and better heat conduction between fluid and solid. A weak Lennard-Jones potential is applied between carbon atoms belonging to the different graphene layers to hold them together at 0.34 nm distance. All Lennard-Jones interactions are truncated at a distance of 1 nm. The channel width, i.e., the distance between the two innermost graphene layers is set to 3.9 nm (roughly 12 molecular diameters) in the *y* direction and periodic boundary

conditions are applied along the x and z directions. The van der Waals size of the carbon atoms (0.34 nm) is subtracted from 3.9 nm to define the available channel width. Room temperature (300 K) is maintained by applying the Nosé-Hoover thermostat to carbon atoms, so that the heat produced by the slip and viscous friction in the water is conducted away through the graphene as is done in a real experiment. The water density in the channel is kept at 1000 kg/m^3. Simulation time spans are from 5 to 10 ns with a time step of ∼1 fs using the leapfrog integration algorithm.

III. RESULTS

A. EMD simulations

We refer to Hansen *et al.*[51] for details on the method of calculating the friction coefficient. In brief, we choose a water slab of width one molecular diameter close to the graphene wall.[47,59] After equilibration, we evaluate the x direction wall-slab shearing force via

$$F'_x(t) = \sum_{\substack{i \in \text{slab} \\ j \in \text{wall}}} F_{ij,x}(t) \tag{1}$$

and the centre of mass (CM) velocity of the slab via

$$u_{\text{slab}}(t) = \frac{1}{m} \sum_{i \in \text{slab}} m_i v_{i,x}(t), \tag{2}$$

where $F_{ij,x}$ is the force on a slab water molecule i due to the carbon atom j at time t (the carbon-oxygen van der Waals force), $v_{i,x}$ is the x-component of the velocity of the slab water molecule i and m is the total mass of the slab $m = \sum_{i \in \text{slab}} m_i$. Using these two quantities, we evaluate the slab velocity-force cross correlation function $C_{uF'_x}(t)$ and slab velocity autocorrelation functions $C_{uu}(t)$

$$C_{uF'_x}(t) = \langle u_{\text{slab}}(0) F'_x(t) \rangle \quad \text{and} \quad C_{uu}(t) = \langle u_{\text{slab}}(0) u_{\text{slab}}(t) \rangle. \tag{3}$$

The Laplace transforms, $\widetilde{C}_{uF'_x}(s)$ and $\widetilde{C}_{uu}(s)$, are then related via the constitutive equation[51]

$$\widetilde{C}_{uF'_x}(s) = -\widetilde{\zeta}(s) \widetilde{C}_{uu}(s). \tag{4}$$

The zero frequency coefficient, ζ_0, is found via the fit between the above two Laplace transformed correlation functions assuming that $\widetilde{\zeta}(s)$ is a Maxwellian memory function. Finally, the friction coefficient, ξ_0, is calculated by dividing

ζ_0 by the surface area of the graphene A. We again refer to Hansen *et al.*[51] for full details of the steps involved. Our result for the friction coefficient between water and graphene is $(1.25 \pm 0.10) \times 10^4$ kg m^{-2} s^{-1}.

The Navier[60] slip length is defined as

$$L_s = \frac{\eta_0}{\xi_0}. \tag{5}$$

Using the bulk water shear viscosity $\eta_0 = (7.5 \pm 0.5) \times 10^{-4}$ kg m^{-1} s^{-1}, the slip length of water on a planar graphene surface is thus estimated as 60 ± 6 nm.

B. NEMD simulations

We perform both Poiseuille and Couette flow NEMD simulations for a wide range of external fields and shear rates starting from the lowest possible values. Poiseuille flow is generated by applying a constant external field to all the atoms of the water molecules and Couette flow is generated by moving the upper graphene wall with a constant velocity while keeping the lower graphene wall fixed. We fit the Poiseuille flow velocity profiles to a quadratic equation $u_x(y) = ay^2 + b$ and Couette flow velocity profiles to a linear equation $u_x(y) = ay + b$ (see Fig. 1). Using these fits one can determine the slip velocity and the fluid velocity gradient at the wall. From these two quantities the NEMD slip length can be found via

$$u_s = L_s \left. \frac{\partial u_x}{\partial y} \right|_{y=y_w}, \tag{6}$$

see Fig. 1. The slip length and friction coefficient are both intrinsic properties of the fluid-solid interface and are independent of the flow type.

1. Couette flow

To our knowledge Couette flow type simulations have not previously been carried out on the water-graphene system in order to determine the slip length. We move the upper wall with a constant velocity in the range 5 to 1000 m/s. Within this range, linearity is expected to hold over a small range of low fluid velocities, above which the slip length is no longer a constant. Even the lowest applied shear rate (wall velocity divided by channel width) is 3 to 4 orders of magnitude higher than the highest experimental shear rate.[61] When we have a small slip system, we can use low wall velocities as the wall
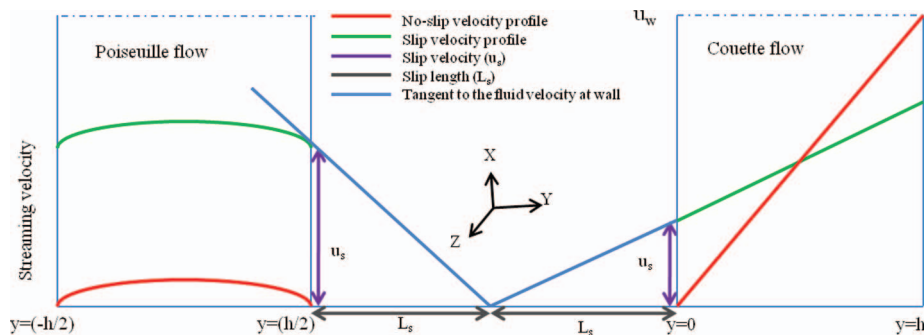

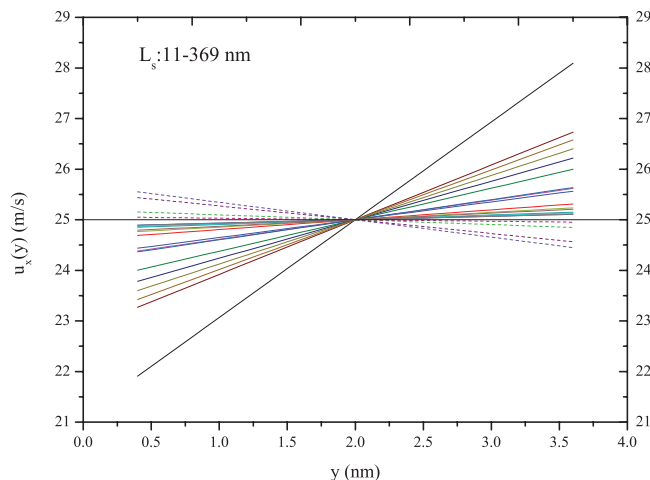FIG. 1. Definitions of slip length and slip velocity for Poiseuille and Couette flows.

FIG. 2. Linear fits to Couette flow velocity profiles at upper wall velocity 50 m/s for the 20 independent simulations. The 4 dotted velocity profiles cannot be used to calculate the slip length (see method-C1). For the other 16 profiles, the slip length varies between 11 and 369 nm.

FIG. 3. Average velocity of 20 independent Couette flow simulations at upper wall velocity 50 m/s with error bars and linear fit. With slip velocity 24.3 ± 0.7 m/s and shear rate $(0.4 \pm 0.4) \times 10^9$ s^{-1}, the predicted slip length using Eq. (6) is 61 ± 55 nm (method-C2).

can induce a measurable fluid flow in the shearing direction. For high slip systems, the difference in wall to fluid velocity increases, so the momentum transfer between wall and fluid decreases, i.e., higher wall velocity is required to induce a measurable fluid flow.

In Fig. 2 we plot the fits to 20 independent simulations, after symmetrizing[62] the streaming velocity data at wall velocity 50 m/s, which is 10 times higher than the smallest velocity we have used. As mentioned earlier, with increasing wall velocity we obtain statistically better NEMD data. We can notice four things from the graph. (i) We have a reasonably good estimate of the average slip velocity ($u_s = 24.3 \pm 0.7$ m/s). (ii) The average velocity difference of the fluid from upper to lower wall is very small ($\delta v \simeq 1.4$ m/s, with the no-slip BC it is 50 m/s). (iii) The fluid strain rate (velocity gradient or slope of the line) is very small and the variation is large among different fits. (iv) Some of the fits have a negative velocity gradient due to the thermal fluctuations superimposed on the very small velocity difference (very weak effective strain rate) which is a result of very strong slip. The standard error in the NEMD simulation streaming velocity data is generally on the order of m/s, which means that for the current system, δv is comparable with the standard error in the velocity data. The number of simulation steps for each independent simulation is 5×10^6 ($t = 5$ ns, $dt = 1$ fs) which is higher than most previous simulation studies of water in carbon nanopores. Each simulation took about 325 hours of central processing unit (CPU) time, i.e., we should expect that from a simulation point of view the velocities are reasonable. We calculate the slip length from the NEMD data in different ways using Eq. (6) as follows.

C1. The general way is to calculate the slip length for all the 20 profiles and then perform the error analysis on this set of 20 independent slip lengths. As mentioned above, some of the velocity fits have negative slope (fluid velocity at the lower wall is greater than at upper wall). For these negative slope profiles the slip len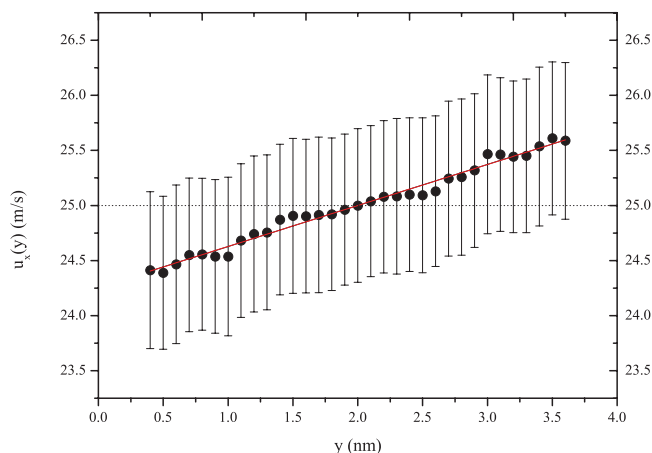gth cannot be defined. Using this procedure we cannot estimate the average slip length. If we disregard these data and only use positive slope velocities to calculate the slip length, it varies from 11 to 369 nm due to the large variation in the velocity gradient.

C2. In this second method, we average the 20 NEMD velocity profiles, and use this averaged data for fitting. In Fig. 3 we plot the averaged NEMD data with error bars and weighted errors method for the fit. The standard error in the NEMD data is approximately equal to the average velocity difference at the walls. Using the method of weighted errors for the fitting, the calculated slip length is 65 ± 2 nm. (Without including the NEMD data errors in the fit (unweighted), the slip length is also 65 ± 2 nm). However, this method underestimates the standard error in the slip length. We have a good estimate of the slip velocity (24.3 ± 0.7 m/s) but not the slope even though the slope is calculated from the velocity, since the slope is very small. The fluid velocity at lower and upper walls is 24.3 ± 0.7 m/s and 25.7 ± 0.7 m/s, respectively. From this, the maximum to minimum slope (strain rate) varies between $(26.4–23.6)/(3.56 \times 10^{-9}) = 0.4 \times 10^9$ s^{-1} and $(25.0–25.0)/(3.56 \times 10^{-9}) = 0 \times 10^9$ s^{-1} ($h = 3.56$ nm being the available channel width). With the slip velocity 24.3 ± 0.7 m/s and strain rate $(0.4 \pm 0.4) \times 10^9$ s^{-1}, the calculated slip length is thus 61 ± 55 nm.

In Fig. 4 we plot the average NEMD data and the corresponding fits for wall velocities of 5 to 60 m/s along with the slip length. For sufficiently small velocities, the slip length is expected to be constant and around 60 nm (our EMD prediction). Due to statistical variations, some anomalous results occurred. For example, at wall velocity 20 m/s, due to the very weak effective strain rates, the average velocity profile across the channel become flat resulting in a slip length in the order of 2 μm. The computed slip length is also inconsistent with the shear rate. So this method is also not reliable in estimating the slip length. At higher wall velocities 70, 80, 90, 100, 125, 150, 200, 250, 300, 500, 750 and 1000 m/s the slip length is 78, 74, 75, 76, 65, 89, 93, 106, 97, 113, 110, 115 nm, respectively.
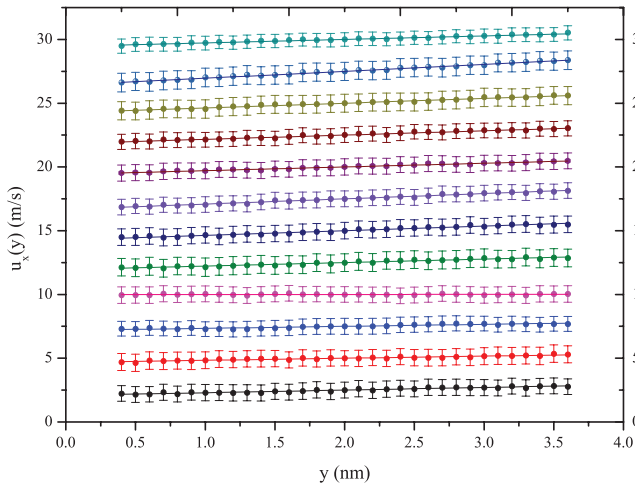
FIG. 4. Same as in Fig. 3 for wall velocity range 5 to 60 m/s with an increment of 5. At the wall velocity 20 m/s, the velocity profile is flat across the channel due to statistical fluctuations and very weak effective strain rate, resulting in a slip length in the order of 2 μm (method-C2).
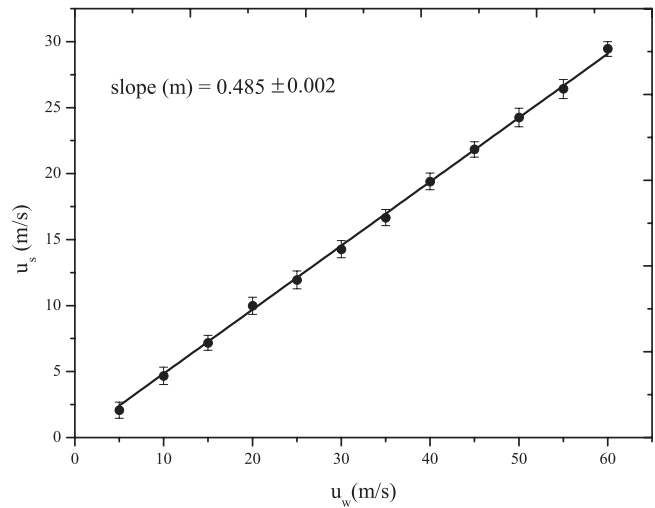

FIG. 5. Slip velocity as a function of wall velocity for low slip velocities where the slip length is expected to be constant. The slip length calculated using Eqs. (9) and (10) is 58 ± 8 nm, with the slope 0.485 ± 0.002 (method-C3).

C3. The classical solution for the velocity profile in Couette flow with the no-slip boundary condition is

$$u_x(y) = \frac{Uy}{h} \ . \tag{7}$$

The fluid velocity at the lower wall ($y = 0$) is zero as it is stationary and at the upper wall ($y = h$) it is equal to the wall velocity U (see Fig. 1). In the case of slip flow, the fluid has a finite velocity u_s at the lower wall and $U - u_s$ at the upper wall. The Couette flow solution with these boundary conditions is

$$u_x(y) = \left(\frac{U - 2u_s}{h}\right) y + u_s \ . \tag{8}$$

Using the slip length definition, Eqs. (5) and (6) we can derive

$$u_s = \left(\frac{L_s}{h + 2L_s}\right) U \ \text{ and } \ u_s = \left(\frac{\eta_0}{\xi_0 h + 2\eta_0}\right) U \ , \tag{9}$$

which means, in the linear regime, where the slip length (friction coefficient) remains constant, the slip velocity is proportional to wall velocity. By plotting slip velocity against wall velocity for low wall velocities we can then find a slope m that enables us to find the slip length. If the no-slip boundary condition holds the slope is zero as the slip velocity is zero irrespective of the wall velocity. As the slip for different wall-fluid systems increases, this slope also increases. The maximum slope value can be close to 0.5 and it should always be less than 0.5. From this slope value, the slip length or friction coefficient can be calculated directly

$$L_s = \left(\frac{mh}{1 - 2m}\right) \ \text{ and } \ \xi_0 = \frac{\eta_0}{h}\left(\frac{1}{m} - 2\right) \ . \tag{10}$$

As m goes to 0.5, the friction coefficient goes to zero and the slip length goes to infinity. In Fig. 5 we plot slip velocity as a function of wall velocity for wall velocities below 60 m/s. The slip velocity is calculated using the method-C2 described above. The slope of the line is 0.485 ± 0.002, which is close to 0.5 as the slip is very strong and the slip velocity is close

to half of the wall velocity. Using this slope (with zero intercept), the slip length is 58 ± 8 nm. To extract this, we have used $10 \times 20 = 200$ simulations each with 325 h of CPU time. The estimated slip length is in agreement with our EMD prediction. Notice, even a 1% increase in the slope leads to a very high slip length as the slip length approaches infinity quickly as m goes to 0.5.

2. Poiseuille flow

For Poiseuille flow we increase the length of the simulations from 5×10^6 to 10×10^6 time steps (10 ns). The external fields range from 0.25×10^{11} to 20.0×10^{11} m/s². The lowest field we used results in $\simeq 3.5$ m/s mean velocity, which is well below the molecular thermal velocity and smaller than the previous simulations mean velocities. Here also, the slip length is expected to be a constant for low field ranges (low slip velocities).

In Fig. 6 we plot the fits of a quadratic equation to the 20 simulations, using symmetrized streaming velocity data at field 1.00×10^{11} m/s². This corresponds to a pressure gradient of 1×10^{14} Pa/m, which is equal to the pressure gradient used by Thomas and McGaughey[29] and the average streaming velocity is also comparable with their Fig. 5 (note that their figure shows the streaming velocity of water in a CNT). Again we note the following observations. (i) We have a good estimate of the average slip velocity (14.7 ± 0.4 m/s). (ii) The average velocity difference of water from the centre to the wall is very small (<0.25 m/s). (iii) The fluid strain rate (velocity gradient) at the wall is very small and the variation is large among different fits. (iv) Some fits are an inverted parabola, which again is the result of statistical fluctuations. The latter point is due to the very small velocity difference from the centre of the channel to the wall (very weak effective strain rate). In Poiseuille flow, as we increase the external field, the fluid velocity difference from the centre to the wall increases (see Eqs. (11) and (12)). Even though these fields are 3 to 4 orders
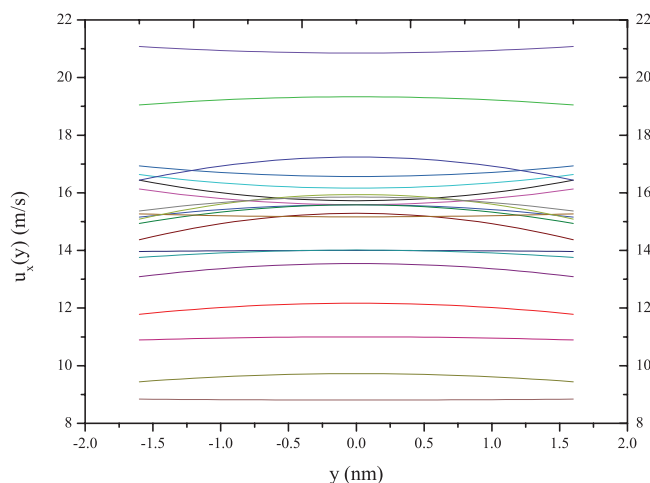
FIG. 6. Quadratic fits to the Poiseuille flow velocity profiles at external field 1.00×10^{11} m/s^2 for the 20 independent simulations. Inverted parabola fits cannot be used to determine the slip length. For the other profiles slip length vary between 10 and 268 nm (method-P1).

of magnitude higher than typical experimental fields, they are still very small for NEMD simulations. At high fields, we can see a clear strongly quadratic velocity profile. In addition to the above mentioned three methods for Couette flow analysis, we use two more methods to calculate the slip length from this NEMD data.

P1. Again compute the slip length for each simulation run separately and then average the slip lengths. For the weak velocity profiles (inverted parabola) the slip length cannot be defined, so this method cannot be used to calculate the average slip length. For the other profiles, the slip length varies between 10 and 268 nm.

P2. We now average the NEMD data over the 20 simulations, and fit the average data. See Ref. 63 for the streaming velocity profiles in the literature. In Fig. 7 we plot the average data with error bars and weighted errors method for fits at fields 1.00×10^{11}, 1.25×10^{11}, and 1.50×10^{11} m/s^2 (note this figure also includes an additional constrained fit which we will explain in method-P4). The estimated slip lengths for the three external fields using weighted errors for the fitting are 60 ± 9, 46 ± 3, and 130 ± 21 nm. Without including the NEMD data errors in the fit (unweighted), the slip lengths are the same as that obtained using weighted errors, which means the standard error in the slip length is underestimated. The calculated shear viscosities from the fitting parameters at three fields are $(7.2 \pm 1.0) \times 10^{-4}$, $(5.6 \pm 0.4) \times 10^{-4}$, and $(15.7 \pm 2.5) \times 10^{-4}$ kg m^{-1} s^{-1}, respectively, (shear viscosity of bulk water is $(7.5 \pm 0.5) \times 10^{-4}$ kg m^{-1} s^{-1}).

As the available channel width is 11 molecular diameters (3.56 nm) and the external fields are small, the shear viscosity of water is not expected to change. Non-local effects occur for channel widths of only a few molecular diameters[3] and nonlinear effects occur at high fields.[47] At field 1.00×10^{11} m/s^2 the NEMD viscosity is in excellent agreement with the bulk water shear viscosity and the slip length is also in excellent agreement with our EMD prediction. At field
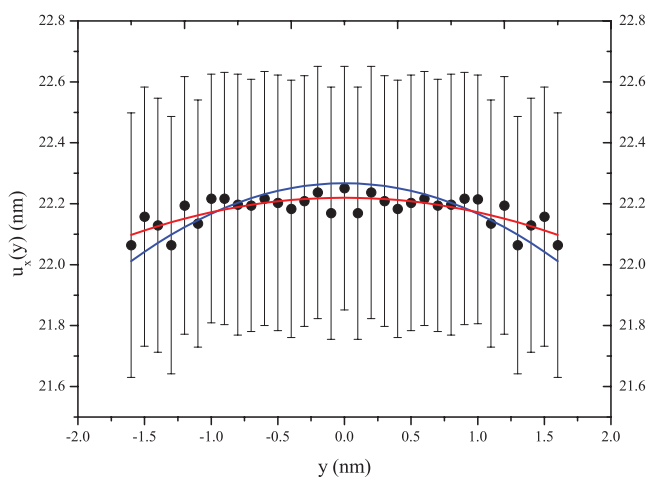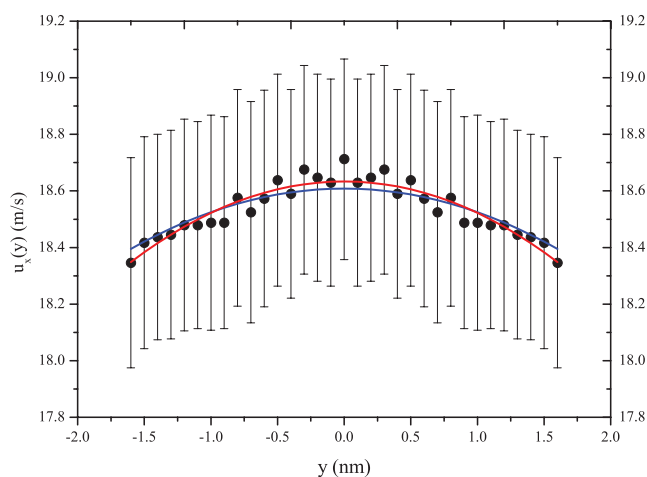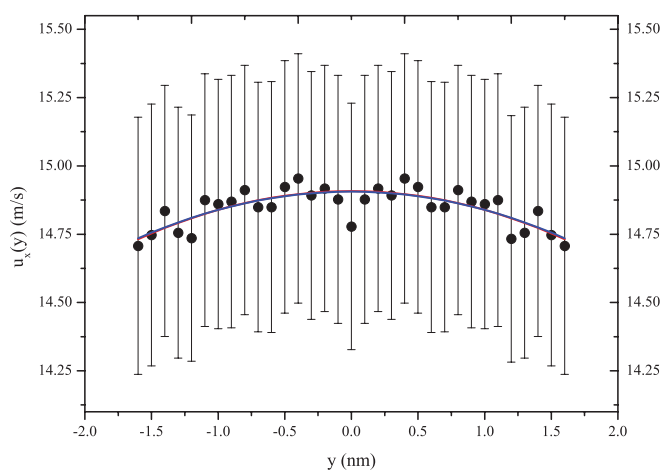

FIG. 7. Average velocity of 20 Poiseuille flow simulations at external fields 1.00×10^{11}, 1.25×10^{11}, and 1.50×10^{11} m/s^2 (from top to bottom) with error bars and both unconstrained fit (red line and method-P2) and constrained fit (blue line and method-P4) with shear viscosity.

1.25×10^{11} m/s^2 the viscosity is underestimated and at field 1.50×10^{11} m/s^2 the viscosity is overestimated. At field 1.25×10^{11} m/s^2 the slip length is underestimated since the viscosity is underestimated (strain rate is overestimated). (see Eq. (6)). At field 1.50×10^{11} m/s^2 we have the opposite behavior, i.e., the viscosity is overestimated resulting in overestimation of the slip length. For the three fields, the slip

velocities are 14.7, 18.3, and 21.9 m/s which are small and hence the shear viscosity and slip length are expected to be constant. This is further explained in method-P3 below.

P3. The Poiseuille flow solution with the no-slip boundary condition is

$$u_x(y) = \frac{\rho F_e}{2\eta_0}\left[\left(\frac{h}{2}\right)^2 - y^2\right]. \tag{11}$$

The fluid velocity at the walls $y = \pm h/2$ is zero and maximum at the centre $y = 0$ (see Fig. 1). The slip modified solution is

$$u_x(y) = \frac{\rho F_e}{2\eta_0}\left[\left(\frac{h}{2}\right)^2 - y^2\right] + u_s, \tag{12}$$

thus the effect of slip is only an upward shift in the velocity profile. Using the slip length definition, Eqs. (5) and (6), we can derive

$$u_s = \left(\frac{L_s \rho h}{2\eta_0}\right) F_e \text{ and } u_s = \left(\frac{\rho h}{2\xi_0}\right) F_e \tag{13}$$

which means, in the linear regime, where the slip length (friction coefficient) remains constant, the slip velocity is proportional to the external field. By plotting slip velocity as a function of external field for low fields we can determine the slope m. Using this slope, the slip length can be directly calculated

$$L_s = \frac{2m\eta_0}{\rho h} \text{ and } \xi_0 = \frac{2m}{\rho h}. \tag{14}$$

Unlike Couette flow, these relations do not suffer from any singularity. In Fig. 8 we plot the slip velocity as a function of external field for low fields (slip velocities). The linear increase in slip velocity with the external field suggests that these external fields are small enough and do not produce nonlinear effects, so the results are applicable to experimental fields also. From the slope the estimated slip length is 63 ± 4 nm which is in agreement with our EMD method prediction.

P4. Unlike the Couette flow solution, the Poiseuille flow solution includes a fluid property (shear viscosity). Thomas and McGaughey[29] found that the unconstrained fit to the velocity profiles resulted in almost 100% deviation in the slip length and shear viscosity from the expected values. In Fig. 7 we plot the constrained fits using the bulk water shear viscosity for the average data of 20 simulations at three external fields 1.00×10^{11}, 1.25×10^{11}, and 1.50×10^{11} m/s^2. The calculated slip length for all the three fields is 62 ± 5 nm. These constrained fit results are also in very good agreement with our EMD prediction. At high fields we notice an increase in temperature of the fluid which also affect the shear viscosity. We have used the shear viscosity at 300 K temperature for the constraining fit. As mentioned before, our goal is to determine the limiting slip length corresponding to experimental fields. If we used a temperature dependent shear viscosity the qualitative behavior of slip would still remain the same at high fields.[47]

P5. The flow enhancement ϵ is defined as the ratio of observed flow rate Q_S in experiments or simulations to that predicted from the classical no-slip boundary condition Q_N. For a planar Poiseuille flow it is related to slip length via

$$\epsilon = \frac{Q_S}{Q_N} = \left(1 + \frac{6L_s}{h}\right). \tag{15}$$

During the NEMD simulations we have counted the number of water molecules crossing a fixed plane in the streaming direction, i.e., we measure the flow rate directly. By dividing this observed flow rate with the Navier-Stokes predicted flow rate, we can directly calculate the flow enhancement at each field. Using this ϵ we calculate the slip length from the above Eq. (15). As this method does not require any fitting to the velocity profiles, it does not suffer from the sensitivity of streaming velocity profiles. In Fig. 9 we have summarized our results and plotted the slip length calculated using
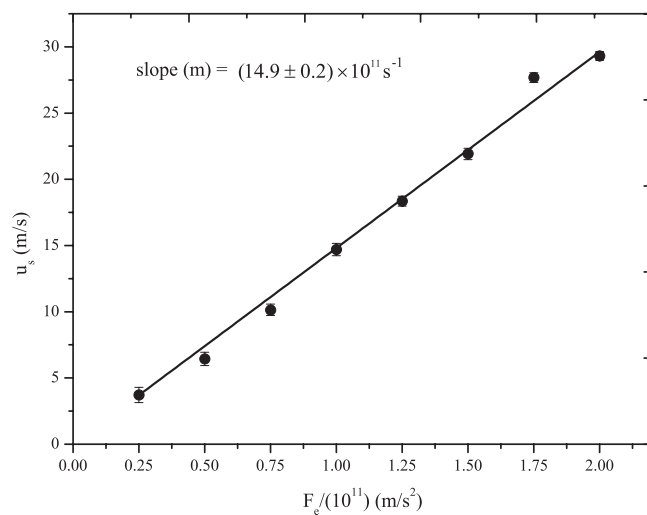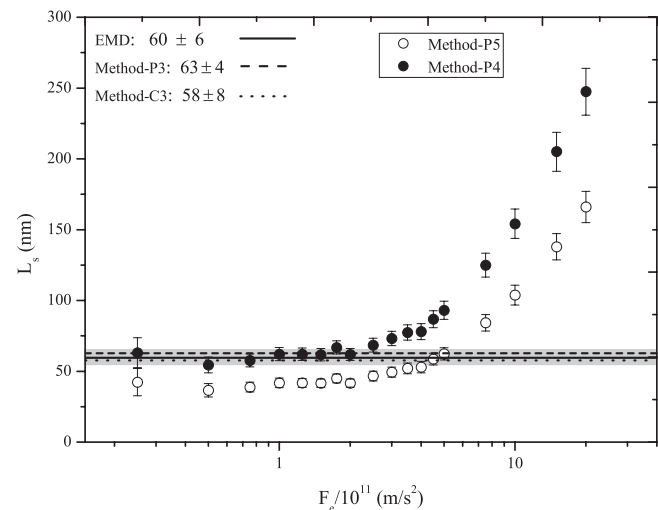

FIG. 8. Slip velocity as a function of external field for low slip velocities for which the slip length is expected to be constant. The predicted slip length calculated using Eqs. (13) and (14) is 63 ± 4 nm, with slope $(14.9 \pm 0.2) \times 10^{11}$ s^{-1} (method-P3).

FIG. 9. Slip length as a function of external field using method-P4 and method-P5. The constant slip length predicted from method-P3 (63 ± 4 nm), method-C3 (58 ± 8 nm), and our EMD prediction (60 ± 6 nm) is also indicated on the graph. The shaded region is the standard error in EMD slip length.

methods-P4 and P5 along with the constant slip length from method-P3, method-C3, and our EMD prediction.

From all the above analysis a good estimate of the slip length is $L_s = 60 \pm 6$ nm. So for the channel width of 3.56 nm used here, the flow enhancement is 102 ± 10 (valid for experimental pressure gradients also).

C. Discussion

In the literature, experimental studies have found up to 400 μm slip length at a planar fluid-solid interface,[64] whereas the slip lengths reported in simulations are in the nm range.[61] We now return to the question: Can a micrometer range slip length be reliably determined using NEMD simulations? On the basis of the analysis above, our answer is "not practical, if not impossible." The reason again is the computational limitations discussed above. NEMD simulations are generally done with a channel width of around 5 nm (15 molecular diameters). For high slip systems, the constant slip length external field/shear rate range shifts to lower values.[47] In a typical shear flow simulation, the upper wall velocity is around 20 m/s and the lower wall velocity is zero. For the slip length to be 1 μm, the fluid velocity at lower and upper walls should be 9.975 and 10.025 m/s, respectively, which means the fluid velocity at the upper wall is just 0.5% higher than the fluid velocity at the lower wall. Using simulations one cannot resolve such a small difference in velocity (0.05 m/s) as the error in the velocity is of the order of m/s. In a channel width of 1 μm, the fluid velocity at the lower and upper walls of 6.66 and 13.33 m/s gives the same 1 μm slip length, but we cannot simulate such a wide channel. In a Poiseuille flow simulation, the slip length remains constant for a very small range of slip velocities. At these small slip velocities, for the slip length to be on the order of a micrometer the fluid velocity gradient has to be too small to determine from NEMD simulations.

Using the integral boundary condition (IBC), one can solve the Navier-Stokes equations for the fluid slab CM velocity for Poiseuille and Couette flow in terms of the friction coefficient. The fluid slab is defined as the first fluid layer close to the wall.[47,51] For Poiseuille flow

$$\langle u_{\text{slab}} \rangle = \frac{\rho F_e L_y}{2\xi_0} , \qquad (16)$$

which is identical to the slip velocity in Eq. (13). For Couette flow, we derive

$$\langle u_{\text{slab}} \rangle = \frac{\eta_0 u_w}{\xi_0(L_y - \Delta) + 2\eta_0} , \qquad (17)$$

which is identical to the slip velocity in Eq. (9) in the limit of the slab width $\Delta \rightarrow 0$.

There is a small uncertainty in defining both the slip velocity and the channel width. Slip velocity is defined as the fluid velocity at the wall as well as the average velocity of the first fluid layer close to the wall. These two definitions are not exactly the same as the fluid remains some distance away from the wall due to the hard core repulsive interactions depending on the type of wall and fluid. There is also uncertainty in defining the channel width. Sometimes it is taken as

the distance between the CM of the solid atoms of the innermost solid layers, sometimes the van der Waals size of the solid atoms (σ) is subtracted from it and at other times the location of the first minimum of the fluid density profile near the wall is considered as the effective wall position.

The matching of the IBC slab velocity using the friction coefficient with the slip modified Navier-Stokes solutions is another confirmation of the validity of our EMD based friction coefficient method. We note that our method has successfully predicted the slip for a variety of systems such as simple fluids (Ar and CH_4) confined between molecular crystal walls,[51] in graphene nanochannels,[47] and for water on a graphene surface, where the slip is low ($\sim$1 nm), moderate ($\sim$8 nm), and high ($\sim$60 nm), respectively. Our method can be applied to any complex fluid-solid system to predict the slip and BC accurately.

The computational time required to calculate the friction coefficient from the EMD method is equal to the time required to generate just one NEMD data point at low fields on Fig. 9 which is $20 \times 650 = 13\,000$ h of CPU time. For determination of friction coefficient by NEMD methods, this time is repeated for each data point, e.g., in Fig. 9, this amounts to roughly an order of magnitude increase in CPU time.

IV. CONCLUSION

Using flexible models for both water and graphene, we have conducted molecular dynamics simulations to precisely quantify the slip length of water on graphene and formulate a BC for water-graphene nanofluidic systems. Slip is found to be extremely sensitive to the NEMD velocity profiles, and the NEMD results suffer from large statistical errors. As demonstrated, the generally used NEMD methods are found to be inaccurate and therefore unreliable in the case of high slip systems, which could be a reason for the disagreement in previous simulation results. We have shown that great care needs to be taken in analyzing the results of NEMD slip data for high-slip systems and have suggested some procedures to increase the reliability of the slip estimates.

On the other hand, one can predict such a highly sensitive non-equilibrium phenomenon with our equilibrium simulation method, accurately and computationally efficiently. With a single set of EMD simulations, one can determine the interfacial friction coefficient between the fluid and solid, and the slip length and overcome the limitations of NEMD methods. The observed high slip can have many potential implications for nanofluidic devices. Water can be a good lubricant for graphene in shearing experiments and graphene nanochannels can act as an efficient water transport device either for enhanced flow or energy saving flow. Extension of the model to cylindrical systems and fluid flow in CNTs is in progress.[52]

[1] W. Sparreboom, A. van den Berg, and J. C. T. Eijkel, Nat. Nanotechnol. **4**, 713 (2009).

[2] G. M. Whitesides, Nature (London) **442**, 368 (2006).

[3] B. D. Todd and J. S. Hansen, Phys. Rev. E **78**, 051202 (2008).

[4] B. D. Todd, J. S. Hansen, and P. J. Daivis, Phys. Rev. Lett. **100**, 195901 (2008).

[5] A. Martini, H.-Y. Hsu, N. A. Patankar, and S. Lichter, Phys. Rev. Lett. **100**, 206001 (2008).

[6] A. E. Kobryn and A. Kovalenko, J. Chem. Phys. **129**, 134701 (2008).

[7] K. P. Travis, B. D. Todd, and D. J. Evans, Phys. Rev. E **55**, 4288 (1997).

[8] C. Neto, D. R. Evans, E. Bonaccurso, H.-J. Butt, and V. S. J. Craig, Rep. Prog. Phys. **68**, 2859 (2005).

[9] S. Kar, R. C. Bindal, S. Prabhakar, P. K. Tiwari, K. Dasgupta, and D. Sathiyamoorthy, Int. J. Nucl. Desalin. **3**, 143 (2008).

[10] T. A. Hilder, D. Gordon, and S.-H. Chung, Small **5**, 2183 (2009).

[11] H. Verweij, M. Schillo, and J. Li, Small **3**, 1996 (2007).

[12] M. Majumder, N. Chopra, R. Andrews, and B. J. Hinds, Nature (London) **438**, 44 (2005).

[13] J. K. Holt, H. G. Park, Y. Wang, M. Stadermann, A. B. Artyukhin, C. P. Grigoropoulos, A. Noy, and O. Bakajin, Science **312**, 1034 (2006).

[14] M. Whitby and N. Quirke, Nat. Nanotechnol. **2**, 87 (2007).

[15] S. Sinha, M. P. Rossi, D. Mattia, Y. Godotsi, and H. H. Bau, Phys. Fluids **19**, 013603 (2007).

[16] M. Whitby, L. Cagnon, M. Thanou, and N. Quirke, Nano Lett. **8**, 2632 (2008).

[17] A. Maali, T. C. Bouhacina, and H. Kellay, Appl. Phys. Lett. **92**, 053101 (2008).

[18] X. Qin, Q. Yuan, Y. Zhao, S. Xie, and Z. Liu, Nano Lett. **11**, 2173 (2011).

[19] M. Majumder, N. Chopra, and B. J. Hinds, ACS Nano **5**, 3867 (2011).

[20] Z. Wang, L. Ci, L. Chen, S. Nayak, M. P. Ajayan, and N. Koratkar, Nano Lett. **7**, 697 (2007).

[21] G. Hummer, J. C. Rasaiah, and J. P. Noworyta, Nature (London) **414**, 188 (2001).

[22] A. Kalra, S. Garde, and G. Hummer, Proc. Natl. Acad. Sci. U.S.A. **100**, 10175 (2003).

[23] E. M. Kotsalis, J. H. Walther, and P. Koumoutsakos, Int. J. Multiphase Flow **30**, 995 (2004).

[24] S. C. Kassinos, J. H. Walther, E. Kotsalis, and P. Koumoutsakos, Lect. Notes Comput. Sci. Eng. **39**, 215 (2004).

[25] I. Hanasaki and A. Nakatani, J. Chem. Phys. **124**, 144708 (2006).

[26] S. R. Majumder, N. Choudhury, and S. K. Ghosh, J. Chem. Phys. **127**, 054706 (2007).

[27] B. Corry, J. Phys. Chem. B **112**, 1427 (2008).

[28] S. Joseph and N. R. Aluru, Nano Lett. **8**, 452 (2008).

[29] J. A. Thomas and A. J. H. McGaughey, Nano Lett. **8**, 2788 (2008).

[30] J. A. Thomas and A. J. H. McGaughey, Phys. Rev. Lett. **102**, 184502 (2009).

[31] X. Chen, G. Cao, A. Han, V. K. Punyamurtula, L. Liu, P. J. Culligan, T. Kim, and Y. Qiao, Nano Lett. **8**, 2988 (2008).

[32] K. Falk, F. Sedlmeier, L. Joly, R. R. Netz, and L. Bocquet, Nano Lett. **10**, 4067 (2010).

[33] J. S. Babu and S. P. Sathian, J. Chem. Phys. **134**, 194509 (2011).

[34] E. M. Kotsalis, "Multiscale modeling and simulation of fullerenes in liquids," Ph.D. dissertation (ETH, Zurich, 2006).

[35] M. D. Ma, L. Shen, J. Sheridan, J. Z. Liu, C. Chen, and Q. Zheng, Phys. Rev. E **83**, 036316 (2011).

[36] T. B. Sisan and S. Lichter, Microfluid. Nanofluid. **11**, 787 (2011).

[37] M. Groombridge, M. Schneemilch, and N. Quirke, Mol. Simul. **37**, 1023 (2011).

[38] T. A. Hilder and J. M. Hill, J. Nanosci. Nanotechnol. **9**, 1403 (2009).

[39] Y. Liu and Q. Wang, Phys. Rev. B **72**, 085420 (2005).

[40] Y. Liu, Q. Wang, T. Wu, and L. Zhang, J. Chem. Phys. **123**, 234701 (2005).

[41] F. Zhu, E. Tajkhorshid, and K. Schulten, Biophys. J. **83**, 154 (2002).

[42] T. Werder, J. H. Walther, R. L. Jaffe, T. Halicioglu, and P. Koumoutsakos, J. Phys. Chem. B **107**, 1345 (2003).

[43] T. G. Myers, Microfluid. Nanofluid. **10**, 1141 (2011).

[44] V. P. Sokhan, D. Nicholson, and N. Quirke, J. Chem. Phys. **117**, 8531 (2002).

[45] Y. Zhu and S. Granick, Phys. Rev. Lett. **87**, 096105 (2001).

[46] D. C. Tretheway and C. D. Meinhart, Phys. Fluids **14**, L9 (2002).

[47] S. K. Kannam, B. D. Todd, J. S. Hansen, and P. J. Daivis, J. Chem. Phys. **135**, 144701 (2011).

[48] S. Bernardi, B. D. Todd, and D. J. Searles, J. Chem. Phys. **132**, 244706 (2010).

[49] V. P. Sokhan, D. Nicholson, and N. Quirke, J. Chem. Phys. **115**, 3878 (2001).

[50] V. P. Sokhan and N. Quirke, Phys. Rev. E **78**, 015301(R) (2008).

[51] J. S. Hansen, B. D. Todd, and P. J. Daivis, Phys. Rev. E **84**, 016313 (2011).

[52] S. K. Kannam, B. D. Todd, J. S. Hansen, and P. J. Daivis, "Hydrodynamic boundary condition for carbon nanotubes" (unpublished).

[53] G. Raabe and R. J. Sadus, J. Chem. Phys. **126**, 044701 (2007).

[54] Y. Wu, H. L. Tepper, and G. A. Voth, J. Chem. Phys. **124**, 024503 (2006).

[55] J. S. Hansen, H. Bruss, B. D. Todd, and P. J. Daivis, J. Chem. Phys. **133**, 144906 (2010).

[56] D. W. Brenner, O. A. Shenderova, J. A. Harrison, S. J. Stuart, B. Ni, and S. B. Sinnott, J. Phys.: Condens. Matter **14**, 783 (2002).

[57] D. Wolf, P. Keblinski, S. R. Phillpot, and J. Eggebrecht, J. Chem. Phys. **110**, 8254 (1999).

[58] C. J. Fennel and J. D. Gezelter, J. Chem. Phys. **124**, 234104 (2006).

[59] A. Niavarani and N. V. Priezjev, Phys. Rev. E **77**, 041606 (2008).

[60] C. L. M. H. Navier, Mem. Acad. Sci. Inst. Fr. **6**, 389 (1823).

[61] E. Lauga, M. P. Brenner, and H. A. Stone, *Experimental Fluid Dynamics* (Springer, New York, 2007).

[62] In Couette flow, if the fluid velocity at a plane is u then the velocity opposite to the centre is $u_w - u$. (see Eqs. (7) and (8)). To highlight the negative velocity gradient we use this fact to symmetrize the velocity profile across the channel. This, in another words, is equivalent to constraining the velocity fit to give $u_w/2$ velocity at the centre of the channel.

[63] The Poiseuille flow velocity profiles of water in CNTs can be seen in Figures 2, 4–5, 1, 5, 1, and 4 in Refs. 23, 25, 28, 29, 31, and 32-supporting information, respectively. Also see Figure 5 in Ref. 44.

[64] C. Lee and C.-J. Kim, Langmuir **25**, 12812 (2009).